Imaging the Surface of Altair

John D. Monnier[1*], M. Zhao[1], E. Pedretti[2], N. Thureau[3], M. Ireland[4], P. Muirhead[5], J.-P. Berger[6], R. Millan-Gabet[7], G. Van Belle[7], T. ten Brummelaar[8], H. McAlister[8], S. Ridgway[9], N. Turner[8], L. Sturmann[8], J. Sturmann[8], D. Berger[1]

[1]Department of Astronomy, University of Michigan, 500 Church Street, Ann Arbor, MI 48109, USA
[2]University of St. Andrews, Scotland, UK
[3]University of Cambridge, Cambridge, UK
[4]California Institute of Technology, Pasadena, CA
[5]Cornell University, Ithaca, NY
[6]Laboratoire d'Astrophysique de Grenoble, France
[7]Michelson Science Center, Pasadena, CA
[8]CHARA, Georgia State University, Atlanta, GA
[9]National Optical Astronomy Observatory, Tucson, AZ
[*]To whom correspondence should be addressed; E-mail: monnier@umich.edu.

Spatially resolving the surfaces of nearby stars promises to advance our knowledge of stellar physics. Using optical long-baseline interferometry, we present here a near-infrared image of the rapidly rotating hot star Altair with $<$1 milliarcsecond resolution. The image clearly reveals the strong effect of gravity darkening on the highly-distorted stellar photosphere. Standard models for a uniformly rotating star can not explain our results, requiring differential rotation, alternative gravity darkening laws, or both.

While solar astronomers can take advantage of high-resolution, multi-wavelength, real-time

imaging of the Sun's surface, stellar astronomers know most stars, located parsecs or kiloparsecs away, as simple points of light. To discover and understand the novel processes around stars unlike the Sun, we must rely on stellar spectra averaged over the entire photosphere. Despite their enormous value, spectra alone have been inadequate to resolve central questions in stellar astronomy, such as the role of angular momentum in stellar evolution (*1*), the production and maintenance of magnetic fields (*2*), the launching of massive stellar winds (*3*), and the interactions between very close binary companions (*4*).

Fortunately, solar astronomers no longer hold a monopoly on stellar imaging. Using long-baseline visible and infrared interferometers, the photospheric diameters of hundreds of stars and high precision dynamical masses for dozens of binaries have been catalogued, offering exacting constraints for theories of stellar evolution and stellar atmospheres (*5*). This work requires an angular resolution of $\sim$1 milliarcseconds (1 part in 2×10^8, or 5 nano-radians) for resolving even nearby stars and is more than an order-of-magnitude better than that achievable with the Hubble Space Telescope or ground-based 8-m class telescopes equipped with adaptive optics.

Stellar imaging can be used to investigate rapid rotation of hot, massive stars. A significant fraction of hot stars are rapid rotators with surface rotational velocities of more than 100 km/s (*6, 7*). These rapid rotators are expected to traverse very different evolutionary paths than their slowly rotating kin (*1*) and rotation-induced mixing alters stellar abundances (*8*). While hot stars are relatively rare by number in the Milky Way Galaxy, they have a disproportional effect on galactic evolution due to their high luminosities, strong winds, and their final end as supernovae (for the most massive stars). Recently, rapid rotation in single stars has been invoked to explain at least one major type of gamma ray bursts (*9*) and binary coalescence of massive stars/remnants for another (*10*).

The distinctive observational signatures of rapid rotation were first described by von Zeipel

(*11*), beginning with the expection that centrifugal forces would distort the photospheric shape and that the resulting oblateness would induce lower effective temperatures at the equator. This latter effect, known as gravity darkening, will cause distortions in the observed line profiles as well as the overall spectral energy distribution. Precise predictions can be made but rely on uncertain assumptions, most critically the distribution of angular momentum in the star – uniform rotation is often assumed for simplicity.

The most basic predictions of von Zeipel theory – centrifugal distortion and gravity darkening – have been confirmed to some extent. The Palomar Testbed Interferometer (PTI) was first to measure photospheric elongation in a rapid rotator, finding the diameter of the nearby A-type star Altair to be $\sim$14% larger in one dimension than the other (*12*). The Navy Prototype Optical Interferometer (NPOI) and the Center For High Angular Resolution Astronomy (CHARA) interferometric array both measured strong limb-darkening profiles for the photometric standard Vega (*13*, *14*), consistent with rapid rotator viewed nearly pole-on. A brightness asymmetry for Altair was also reported by NPOI (*15*, *16*), suggestive of the expected pole-to-equator temperature difference from gravity darkening. In recent years, a total of five rapid rotators have been measured to be elongated by interferometers (*17–19*).

While von Zeipel theory appears to work at a basic level, serious discrepancies between theory and observations have emerged. Most notably, the diameter of the B3V-type star Achernar (*17*) was measured to be $\sim$1.56 times longer in one dimension than the other, too large to be explained by von Zeipel theory. Explanations for this include strong differential rotation of the star (*20*) or the presence of a polar wind (*3*), either of which have far-reaching consequences for our understanding of stellar evolution. In order to address these issues, we must move beyond the simplest models for rapidly rotating stars, and this will require a corresponding jump in the quality and quantity of interferometry data. Indeed, all previous results were based on limited interferometer baselines, lacking the capability to form model-independent images, relying

entirely on model-fitting for interpretation. Thus previous confirmations of von Zeipel theory, although suggestive, were incomplete.

Here we report a development in imaging capabilities that tests the von Zeipel theory, both through basic imaging and precise model-fitting. By combining near-infrared light from four telescopes of the Georgia State University CHARA interferometric array, we have synthesized an elliptical aperture with dimensions 265x195 meters (Figure 1), allowing us to reconstruct images of the prototypical rapid rotator Altair (spectral type A7V) with an angular resolution of $\sim$0.64 milliarcseconds, the diffraction limit defined by $\frac{\lambda}{2D}$, the observing wavelength divided by twice the longest interferometer baseline. The recently-commissioned Michigan Infrared Combiner (MIRC) (*21*) was essential for this work, allowing the light from the CHARA telescopes to be all combined together simultaneously in 8 spectral channels spanning the astronomical H band ($\lambda = 1.50-1.74\mu$m). The Altair data presented here were collected on UT2006Aug31 and UT2006Sep01 – complete observational information is available (*22*). In addition, we utilized some K band ($\lambda = 2.2\mu$m) observations by the PTI to constrain the short-baseline visibilities in subsequent analysis.

By using four CHARA telescopes, interferometric imaging of Altair is now possible, although this requires specialized image reconstruction techniques. We utilized the publicly-available application "Markov-Chain Imager for Optical Interferometry (MACIM)" (*23*) in this work, applying the Maximum Entropy Method (MEM) (*24*). We restricted the stellar image to fall within an elliptical boundary, similar in principle to limiting the field-of-view in standard aperture synthesis procedures. This restriction biases our imaging against faint emission features arising outside the photosphere; however, we do not expect any circumstellar emission in Altair which is relatively cool, lacking signs of gas emission or strong winds. Further details of our imaging procedures, along with results from validation tests, can be found in (*22*).

Our image shows the stellar photosphere of Altair to be well-resolved (Figure 2A), appear-

ing elongated in the NE-SW direction with a bright dominant feature covering the northwest quadrant of the star. In order to reduce the influence of possible low-level artifacts that are beyond the diffraction-limit of our interferometer, we have followed the standard procedure (*25*) of convolving the reconstructed image with a Gaussian beam matching the resolution of the interferometer (Figure 2B).

These images confirm the basic picture of gravity darkening induced by rapid rotation. We see Altair's photosphere to be oblate with a bright region identifiable as the stellar polar region. The intensity of the dark equatorial band is approximately 60-70% of the brightness at the pole, broadly consistent with expectations for the near-infrared from previous models. While we see some evidence for deviations from axisymmetry (small excess emission on northern limb), this feature is at the limit of our image fidelity and will require additional Fourier coverage to investigate further.

We have also fitted our new extensive dataset with a rapid rotator model, following the prescription set out in Aufdenberg et al. (*14*) and references therein, assuming a Roche potential (central point mass) and solid body rotation. The main parameters of the model are the stellar radius and temperature at the pole, the angular rotation rate as a fraction of breakup (ω), the gravity darkening coefficient (β) and the viewing angles (inclination and position angle). We employed the stellar atmosphere models of Kurucz (*26*) for determining the specific intensity of each point on the surface as a function of local gravity, effective temperature, and limb darkening. In addition to matching the new MIRC/CHARA data, we forced the model to match the measured V and H band photometric magnitudes (0.765$\pm$0.015 and 0.235$\pm$0.043 respectively) derived from a broad literature survey. When fixing the gravity-darkening cofficient to $\beta = 0.25$ appropriate for radiative envelopes, our derived parameters (Table 1) agree well with best-fit parameters of Peterson et al. (*15*) based on visible data. However, our best-fit model reached only a reduced χ^2_ν of 1.79, suggesting a need for additional degrees of freedom in our

model.

In order to improve our fits, we explored an extension to the von Zeipel model, allowing the gravity darkening coefficient β to be a free parameter. We found that $\beta = 0.190$ model significantly improved the goodness-of-fit (Table 1) and this improvement is visually apparent when comparing synthetic model images to the Altair image from CHARA (Figure 3). In addition to a lower β, the new model prefers a slightly less inclined orientation, a cooler polar temperature, and a faster rotation rate.

Both our imaging and modeling results point to important deficiencies in the currently-popular models for rapid rotators. Previous workers have also encountered problems explaining high-resolution interferometry data with standard prescriptions for rotating stars. In addition to the Achernar case previously cited, Peterson et al. (*15*) were unable to find a satisfactory fit for Altair assuming a standard Roche - von Zeipel model ($\chi^2_\nu = 3.8$), consistent with the need for additional stellar physics. Recent results for Alderamin (*19*) also specifically favor models with smaller βs, in line with our findings.

While model fitting has revealed deviations from standard theory, our model-independent imaging allows new features to be discovered outside current model paradigms. The most striking difference between our CHARA image and the synthetic model images (Figure 3) is that our image shows stronger darkening along the equator, inconsistent with any von Zeipel-like gravity darkening prescription assuming uniform rotation.

Lower equatorial surface temperatures could naturally arise if the equatorial rotation rate was higher than the rest of the star (differential rotation), reducing the effective gravity at the surface (*27*). Another possibility is that the cooler equatorial layers could be unstable to convection (*28, 29*), invalidating a single gravity darkening "law" applicable to all stellar latitudes. Other studies (*30*) have found further faults with simple application of the von Zeipel law due to opacity effects in the surface layers.

While difficult to isolate or untangle these various effects from one another, nevertheless the new interferometric results and our modeling convincingly establishes the case for stellar physics beyond the standard models used today to describe rotating stars. A path forward is clear: differential rotation will leave both geometric and kinematic signatures different from opacity or convection-related phenomena. Observers must be armed with a new generation of models incorporating these physical processes in order to exploit the powerful combination of detailed line profile analysis and multi-wavelength interferometric imaging now available.

References and Notes

1. A. Maeder, G. Meynet, ARA&A **38**, 143 (2000).
2. J. D. Landstreet, A&A Rev. **4**, 35 (1992).
3. P. Kervella, A. Domiciano de Souza, A&A **453**, 1059 (2006).
4. P. Barai, *et al.*, ApJ **608**, 989 (2004).
5. J. D. Monnier, *Reports of Progress in Physics* **66**, 789 (2003).
6. H. A. Abt, N. I. Morrell, ApJS **99**, 135 (1995).
7. H. A. Abt, H. Levato, M. Grosso, ApJ **573**, 359 (2002).
8. M. Pinsonneault, ARA&A **35**, 557 (1997).
9. G. E. Brown, *et al.*, *New Astronomy* **5**, 191 (2000).
10. N. Gehrels, *et al.*, Nature **437**, 851 (2005).
11. H. von Zeipel, MNRAS **84**, 684 (1924).
12. G. T. van Belle, D. R. Ciardi, R. R. Thompson, R. L. Akeson, E. A. Lada, ApJ **559**, 1155 (2001).
13. D. M. Peterson, *et al.*, Nature **440**, 896 (2006).
14. J. P. Aufdenberg, *et al.*, ApJ **645**, 664 (2006).
15. D. M. Peterson, *et al.*, ApJ **636**, 1087 (2006).
16. N. Ohishi, T. E. Nordgren, D. J. Hutter, ApJ **612**, 463 (2004).

17. A. Domiciano de Souza, *et al.*, A&A **407**, L47 (2003).

18. H. A. McAlister, *et al.*, ApJ **628**, 439 (2005).

19. G. T. van Belle, *et al.*, ApJ **637**, 494 (2006).

20. S. Jackson, K. B. MacGregor, A. Skumanich, ApJ **606**, 1196 (2004).

21. J. D. Monnier, J.-P. Berger, R. Millan-Gabet, T. A. Ten Brummelaar, *SPIE v.5491. (ed. Traub)*, W. A. Traub, ed. (2004), pp. 1370–+.

22. Online Supplemental Materials.

23. M. J. Ireland, J. D. Monnier, N. Thureau, *SPIE v.6268 (eds. Monnier, Schöller, Danchi)* (2006).

24. R. Narayan, R. Nityananda, ARA&A **24**, 127 (1986).

25. J. A. Högbom, A&AS **15**, 417 (1974).

26. R. Kurucz, *ATLAS9 Stellar Atmosphere Programs and 2 km/s grid.* **13** (1993).

27. S. Jackson, K. B. MacGregor, A. Skumanich, ApJS **156**, 245 (2005).

28. A. Claret, A&A **359**, 289 (2000).

29. F. Espinosa Lara, M. Rieutord, *astro-ph/0702255* (2007).

30. C. C. Lovekin, R. G. Deupree, C. I. Short, ApJ **643**, 460 (2006).

31. T. A. ten Brummelaar, *et al.*, ApJ **628**, 453 (2005).

32. D. Erspamer, P. North, A&A **398**, 1121 (2003).

33. M. A. C. Perryman, ESA, *The HIPPARCOS and TYCHO catalogues.* (ESA Publications Division, ESA SP Series vol no: 1200, 1997).

34. We acknowledge contributions from Ajay Tannirkulam, Scott Webster, Andy Boden, Bob Zavala, Chris Tycner, Christian Hummel, Deane Peterson, Jason Aufdenberg, PJ Goldfinger, and Steve Golden. Research at the CHARA Array is supported by the National Science Foundation through grants AST 06-06958 and AST 03-52723 and by the Georgia State University through the offices of the Dean of the College of the Arts and Sciences and the Vice President for Research.

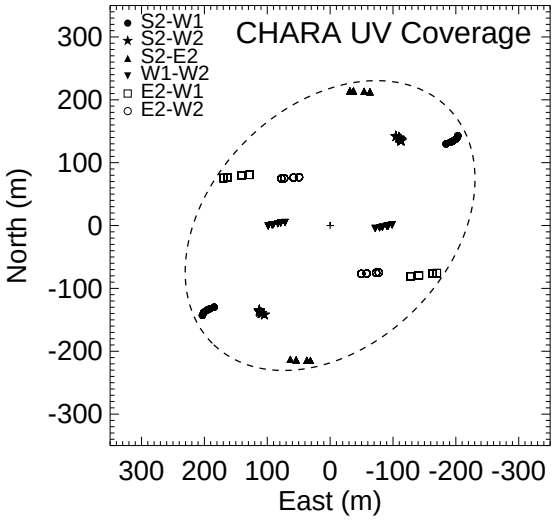

Figure 1: This figure shows the Fourier UV coverage for the Altair observations, where each point represents the projected separation between one pair of CHARA telescopes (S2-E2-W1-W2) (*31*). The dashed ellipse shows the equivalent coverage for an elliptical aperture of 265×195 meters oriented along a Position Angle of 135° East of North.

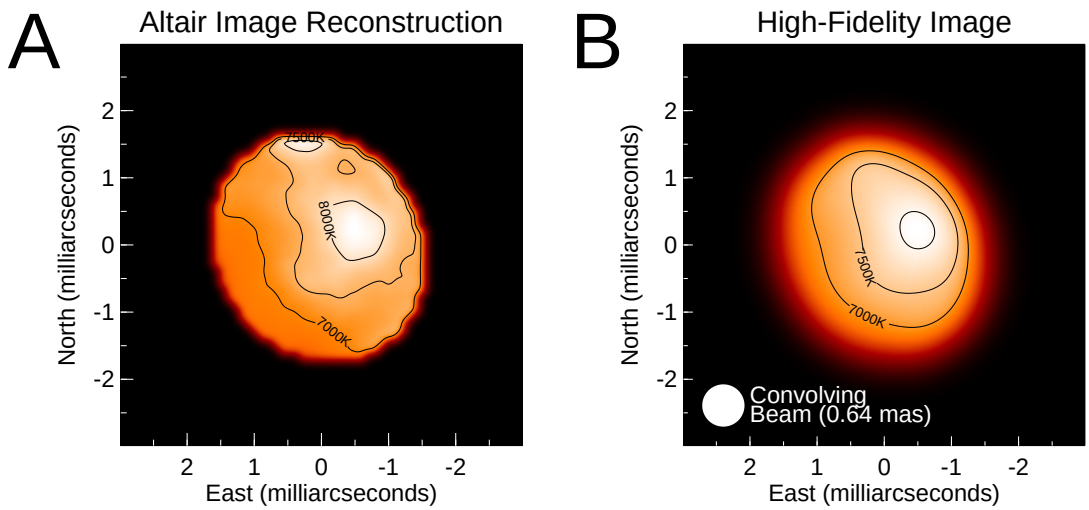

Figure 2: A) shows the intensity image of the surface of Altair ($\lambda = 1.65\mu$m) created with the MACIM/MEM imaging method using a uniform brightness elliptical prior ($\chi^2_\nu = 0.98$). Typical photometric errors in the image correspond to $\pm$4% in intensity. B) shows the reconstructed image convolved with a Gaussian beam of 0.64 mas, corresponding to the diffraction-limit of CHARA for these observations. For both panels, the specific intensities at 1.65μm were converted into the corresponding blackbody temperatures and contours for 7000K, 7500K, and 8000K are shown. North is up and East is left.

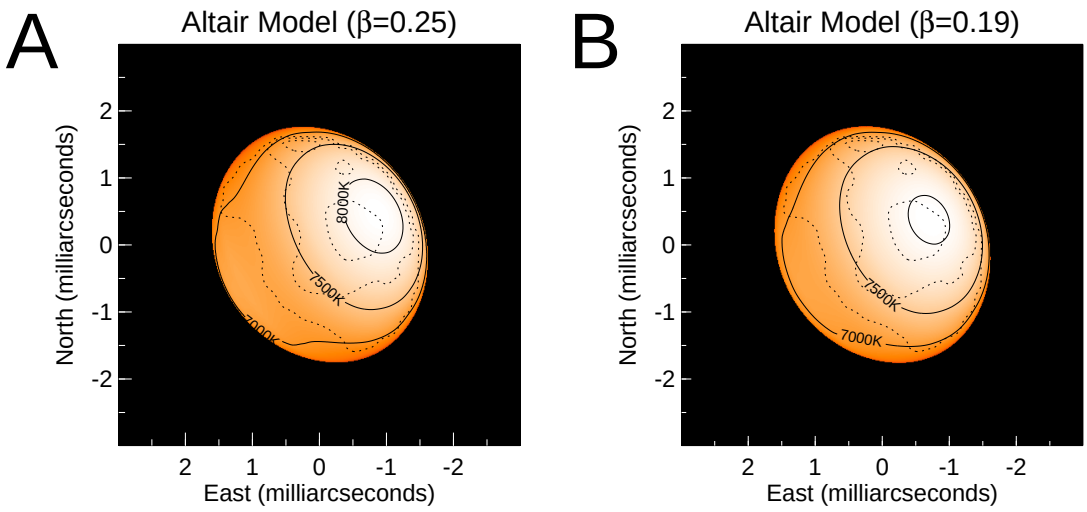

Figure 3: The panels show synthetic images of Altair ($\lambda = 1.65\mu$m) adopting conventional rapid rotation models. A) is the best-fit model assuming standard gravity-darkening coefficient for radiative envelopes ($\beta = 0.25, \chi^2_\nu = 1.79$) while B) shows the result when β is a free parameter ($\beta = 0.190, \chi^2_\nu = 1.37$). For both panels, the specific intensities at 1.65μm were converted into the corresponding blackbody temperatures and contours for 7000K, 7500K, and 8000K are shown. We have overplotted the contours from the CHARA image (Figure 2A) as dotted lines to facilitiate intercomparison.

Table 1: Best-fit parameters for Roche - von Zeipel models of Altair. Parameter descriptions: Inclination (0° is pole-on, 90° is edge-on) & Position Angle (degrees East of North) describe our viewing angle, T_{pole} / R_{pole} describe the temperature and radii of the pole (alternatively, one can describe the temperature and radii at the equator T_{eq} / R_{eq}), ω is the angular rotation rate as a fraction of critical breakup rate, β is the gravity-darkening coefficient. Models assumed stellar mass 1.791 $M_\odot$ (*15*), metallicity [Fe/H]$= -0.2$ (*32*), and distance 5.14 pc (*33*).

Parameters	β Fixed	β Free
Inclination (degs)	62.7 ± 1.5	57.2 ± 1.9
Position Angle (degs)	-61.7 $\pm$ 0.9	-61.8 $\pm$ 0.8
T_{pole} (K)	8710 ± 160	8450 ± 140
R_{pole} ($R_\odot$)	1.661 ± 0.004	1.634 ± 0.011
(mas)	1.503 ± 0.004	1.479 ± 0.010
T_{eq} (K)	6850 ± 120	6860 ± 150
R_{eq} ($R_\odot$)	2.022 ± 0.009	2.029 ± 0.007
(mas)	1.830 ± 0.008	1.835 ± 0.007
ω	0.902 ± 0.005	0.923 ± 0.006
β	0.25 (Fixed)	0.190 ± 0.012
Model V Mag	0.765	0.765
Model H Mag	0.225	0.220
Model v $\sin i$ (km/s)	241	240
Reduced χ^2:		
Total	1.79	1.37
Closure Phase	2.08	1.73
Vis^2	1.48	1.10
Triple Amp	2.14	1.58